Tuning the Optically Bright and Dark States of Doped Graphene Quantum Dots

Madhuri Mukhopadhyay, Bradraj Pandey, and Swapan K. Pati*

Theoretical Sciences Unit, Jawaharlal Nehru Centre for Advanced Scientific Research, Bangalore 560064, India

(Received 5 February 2016; revised manuscript received 6 August 2016; published 24 October 2016)

Employing a combination of the many-body configuration-interaction method described by an extended Hubbard model and first-principles calculations, we predict the emergence of high oscillator strength at the near-IR region which originates from the Davydov type of splitting in doped graphene quantum dots (GQDs). Incorporation of the strain in GQDs promotes closely spaced bright states that are pertinent to coherent excitation. Controlling the destructive interference of the functionalized-nanographene quantum states, the dark states can be tuned towards the red end, ensuring that the system is a good candidate for a photocell. On the other hand, the coherent states can be tailored to concentrate the light at a very high intensity, resulting in an opportunity for a photonic device.

DOI: 10.1103/PhysRevApplied.6.044014

I. INTRODUCTION

With the advancement in the fabrication of atomically thin materials [1–5] and graphene nanoflake-based devices, functionalized-graphene nanoflakes are attracting significant attention due to their promising electronic and optical properties, especially for applications in photonics and solar cells [6–9]. The electronic and optical properties of the graphene-based low-dimensional structures change in a nontrivial manner depending on the shape, the size, and the edges [10–12]. Stacking of the graphene layers controls the optical properties in significant ways. Depending on the angle of the twisted sublayer of the graphene, stacking shifts the energy of the absorption spectra and leads to van Hove singularities [13]. The functionalization of graphene structures changes their properties in dramatic ways [14,15]. For example, graphene is a gapless semimetal, but fully hydrogenated graphene (graphane) has been predicted to have a local-density-approximation gap of 3.4 eV [16].

While graphene is stabilized due to delocalization, its boron-nitrogen analog is a stable Mott insulator due to charge transfer. However, since a B—N bond is isoelectronic with C—C bonds, replacing C with B or N adds a hole or an electron, keeping the structure the same. Hence, graphene was doped with nitrogen and boron in several earlier studies [17,18]. However, reliable control of optoelectronic properties by chemical doping is still a challenging task. Experimentally, one of the most common techniques for the production of doped graphene is the *in situ* introduction of B- (N-) containing precursors during a chemical vapor deposition (CVD) process [19,20].

Other methods have also been used successfully to produce nitrogen doped graphene fragments [21,22]. There have been many works on the optical response of graphene and truncated graphene, i.e., graphene quantum dots (GQDs). For GQDs, the excitonic features are more exotic than in their 2D analog [23,24]. Not only does the geometrical confinement of the GQDs change the optical properties significantly, but the edge states also play a crucial role in introducing some alternative optical and magnetic properties [25–30]. In particular, zigzag-edged GQDs, which display sublattice symmetry breaking, generate the degenerate edge states in the vicinity of the Fermi level. These degenerate edge states give rise to a spin-polarized ground state, which is promising for spintronics applications [31–33].

However, the optical properties due to edge states get significantly modified by the introduction of chemical doping [34]. Our studies also reflect that the low-lying states of GQDs are no longer dictated by their boundary condition; rather, they are controlled by the nature of the chemical doping. Chemical doping can also be a way to introduce dipole-dipole-type interactions in the GQDs, which may regulate their delocalized states. Now, the coherent control of excitonic states over the optical transition is dictated by the linear superposition of quantum states with symmetric or antisymmetric phase matching, resulting in either an addition or a reduction of the electrical transition dipole [35,36]. The dipole-dipole interaction also modulates the charge-density-wave and spin-density-wave phases, which can modify the optical response in a significant way. We have investigated here how the architecture of the B-N substitution in GQDs can govern the Davydov-type splitting [37,38], resulting in coherent control of the excitonic states. The relative position of boron and nitrogen substitution and their partial dipole–partial dipole coupling can perturb the shallow bound exciton of the GQDs and, in some cases, can overwhelm the intrinsic excitonic interaction and can develop high

*pati@jncasr.ac.in

oscillator strength at different energies, making the system interesting for optoelectronic devices. On the other hand, the particular orientation of the partial dipole created by the boron and/or nitrogen substitution can result in low-lying dark states, which can act as a good donor in a photocell composite.

A recent kinetic model study showed that control over the delocalized dark states can enhance photocurrents and maximize power outputs by 35 percent over a classical cell [39,40]. In fact, they utilized the Davydov-type splitting due to the dipole-dipole interactions for the model aggregates, and from the rate of electron transfer, they concluded that enhancement of the photocurrent is due to the dipolar interaction in the aggregates. Here, we ask whether we can control the delocalized states of the graphene quantum dots through the dipolar type of coupling to control the relative position of the bright and dark states, which can be interesting for the photonic device or the photocell either way. In our study, we conduct many-body calculations using the extended Hubbard model, considering the Coulomb-interaction potential and the dipolar coupling. We also carry out first-principles calculations that consider different functionals to study the nonlocal correlations. We show through chemical doping in GQDs that we can control the relative position of the dark and bright states. Our studies predict that, for the functionalized GQDs, the emergence of high oscillator strength can be governed by the partial dipole–partial dipole interaction. Again, the relative position of a dark state compared to its bright counterpart is very important experimentally, as its apparent position can make a dark state either a good electron acceptor or a good electron donor. If a dark state is blueshifted in energy compared to the bright states, it can act as a good electron acceptor for a given electron-enriched system in a photocell composite. On the other hand, a low-lying dark state compared to bright states may get populated by excited electrons through phonon relaxation and can act as an electron donor as well. Hence, the dark-state energy of the GQDs can be tuned relative to another electron donor and/or acceptor system to make the GQDs efficient for photocell applications. Our results provide a comprehensive understanding regarding the relative position of delocalized states of GQDs and suggest guidelines for an experimentalist to dope graphene nanofragments chemically to get the desired properties in a controlled manner.

II. MODELING AND COMPUTATIONAL DETAILS

GQDs are effectively π-conjugated large molecules involving an sp^2 carbon backbone. For our calculations, we have chosen the Pariser-Parr-Pople (PPP) model, as it includes explicit long-range electron-electron interactions and gives a physically consistent and numerically accurate description for these kinds of systems [41]. The extended Hubbard (or PPP) Hamiltonian, together with the dipole-dipole potential, can be written as

$$
\begin{aligned}
H &= \sum_i n_i \varepsilon_i + \sum_{\langle i,j\rangle,\sigma} t_{i,j}(\hat{a}^{\dagger}_{i,\sigma}\hat{a}_{j,\sigma} + \text{H.c.}) + \sum_i U_i n_{i\uparrow} n_{i\downarrow} \\
&\quad + \sum_{i,j} (V^{\text{ppp}}_{i,j} + V^{\text{dipdip}}_{i,j})(n_i - z_i)(n_j - z_j) \\
V^{\text{ppp}}_{i,j} &= 14.397\left[\left(\frac{28.794}{U_i + U_j}\right)^2 + r^2_{ij}\right]^{-(1/2)} \\
V^{\text{dipdip}}_{i,j} &= \frac{(\vec{r}_i)\cdot(\vec{r}_j)}{r^3_{ij}} \qquad (1)
\end{aligned}
$$

(using standard notation) with the configuration-interaction (CI) method. We consider the nearest-neighbor hopping integral t_{ij} to be the same ($t = 1$ eV) for all of the bonds. The on-site Coulomb repulsion, U, is approximated from the difference between the first ionization energy and the electron affinity of an atom and is scaled for carbon, boron, and nitrogen to be 5, 4, and 7 (in units of t), respectively. The on-site energies (ε_i's) for carbon, nitrogen, and boron are scaled as 0, −0.3, and 0.2 (in units of t), respectively. The multideterminantal CI approach is one of the best methods for obtaining excited-state properties [42]. As the CI is developed in molecular-orbital (MO) space instead of real space, one can have control over the promotions of electrons from the filled MOs to the empty MOs. In principle, a full CI is capable of providing exact solutions for all of the ground and excited states. Since the GQDs that we consider are quite large for exact calculations, we use a complete active-space CI method, which is very good for low-energy optical spectra. We consider a small energy window in the MO space, taking all possible configurations of 4900 within the active space close to the ground state.

The long-range Coulomb-interaction potential, V^{ppp}_{ij}, is parametrized in the Ohno interpolation scheme [43], and the dipolar coupling, V^{dipdip}_{ij}, is calculated from the dipolar interactions [44,45]. In our case, instead of molecular dipoles, we consider the partial dipoles to be on the same plane of the GQDs, where n_i and n_j are the number density operators and $\vec{r}_i$, $\vec{r}_j$ are the unit vectors. Thus, the dipolar coupling is dictated by the direction and the angles between the partial dipoles in the GQDs created by boron or nitrogen substitution. This boron or nitrogen doping will modulate the average occupancy calculated by the number operator, resulting in either attractive potential or repulsive potential.

Along with model calculations, we also perform *ab initio* spin-polarized density-functional-theory (DFT) calculations for the systems using the software GAUSSIAN 09 program. Both the Becke, three-parameter, Lee-Yang-Parr (B3LYP) and the long-range corrected (Coulomb-attenuating-method B3LYP) exchange-correlation functional (which also takes into account nonlocal correlation) is used in association with the 6–31 + $g(d)$ basis set for all of the calculations. For large structures, Gaussian Zerner's intermediate neglect of differential overlap (ZINDO) calculations

are also done. We calculate the linear electronic absorption spectra using time-dependent density-functional-theory (TD-DFT) methods. A minimum of ten lowest excited states are considered in each of the studies.

III. RESULTS AND DISCUSSION

The high oscillator strength in the graphene nanoflakes is generated by the linear superposition of different configurations in a manner such that the transition dipoles become macroscopic due to constructive interference of the phase factors of the quantum states [35,36]. On the other hand, the corresponding destructive interference results in a reduction of the transition dipoles, producing dark states, as shown in Fig. 1(a). Figure 1(b) shows the positively interfering coherent peak (β), the negatively interfering destructive peak (α), and the edge-state contributing peak for GQDs with 30 carbon atoms, i.e., polyacene containing seven rings. The main contributing transitions in the absorption spectra are presented in Table I along with

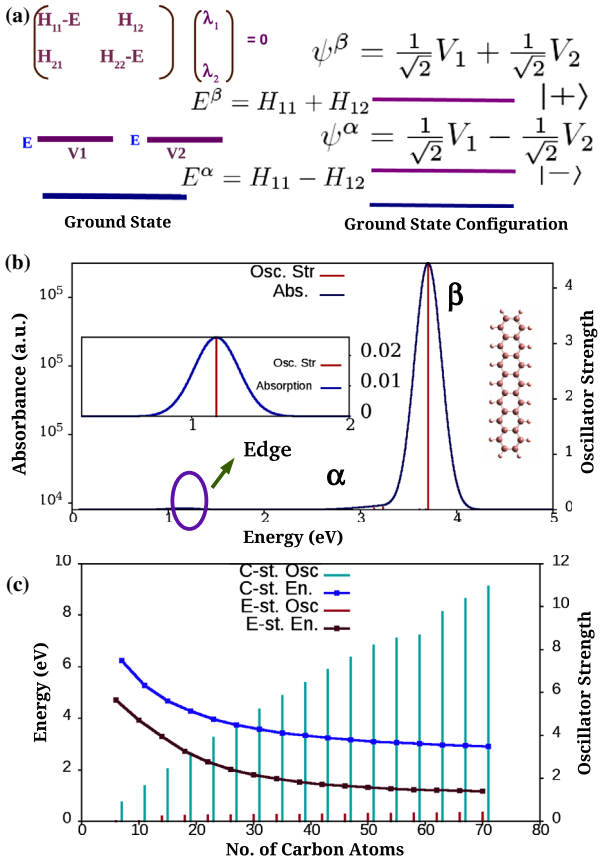

FIG. 1. (a) Schematic of constructive and destructive interfering states. (b) Absorption spectra of C30 acene GQDs calculated by TD-DFT using the B3LYP functional. (Inset) Edge-state absorption. (c) With an increase in size, edge-state absorption energy gets redshifted more steadily compared to coherent-state (β) absorption. For edge states, the oscillator strengths remain more or less the same but, for the coherent states, the strengths increase steadily (when taken from the ZINDO calculation).

the states involved for the transitions, with the probability of the transitions given in parentheses. Table I reflects the coherent sum of the transition-dipole vectors contributing to the high-energy peak (β) (transition-dipole vectors are in the same direction, at high oscillator strength), whereas for the low-energy peak (α) the transition-dipole vectors almost get canceled out (transition-dipole vectors are in the opposing direction, at low oscillator strength). An interesting point is that the lowest energy peak, (shown magnified in the inset) is not like an additive type; rather, it has a contribution from the low-lying states (as shown in Table I, only two states are involved)—often termed as an edge-state transition, as the transition occurs near the Fermi level—which is highly redshifted, making the system near-IR active. The edge-state transitions are, in general, quite interesting, as the optical-gap oscillations in these cases (which have already been reported [46]) originate from a band crossing at the Fermi level. However, the oscillator strength for all of the transitions and its mere presence and the strength of the edge-state transition is often overestimated in DFT and ZINDO calculations [see the Supplemental Material (SM) [47]]. The edge-state effects are less prominent in the armchair analog and in circularly shaped GQDs. In our earlier work, we studied in detail the edge-state transition and how ground-state spin multiplicity plays a crucial role [48]. The main point is that, for all types of GQDs with different edges, the strength of the coherent peak increases with the system size, along with a lowering of the transition energy (see also the SM [47]).

Figure 1(c) shows the difference between the fundamental nature of the coherent peak and the peak generated from the edge-state transition, as the oscillator strengths of the edge states remain more or less unchanged with an increase in the size of the system, while the oscillator strengths of the coherent peaks increase steadily with the system size due to a more and more positive in-phase combination of the transition-dipole vectors of the delocalized states (see the SM [47]).

Now, we believe that an introduction of strain in graphene quantum dots can alter the on-site Coulombic

TABLE I. For C30 acene GQDs, the transition energy, the states involving the transitions (with their percentages of contribution in parentheses), the transition dipoles and their directions, and the resulting oscillator strengths are presented.

Energy (eV)	States involved	Tr. dipole (a.u.)	Osc. str.
3.7 [coherent (β)]	96–100 (43)	0.464 61↑	4.4482
	99–103 (57)	0.535 40↑	
2.9 [incoherent (α)]	96–100 (56)	0.530 46↑	0.0192
	99–103 (42)	−0.457 53↓	
1.2 (edge)	99 to 100 (approx. 100)	0.721 21↑	0.0259
	100 to 99 (negligible)	−0.139 88↓	

interaction. The effect of strain can be utilized to modify the energy and the transition strength of an optical probe. Figure 2(a) shows how transition energy and the transition amplitude depend on the U/t values. With the increase in strain, i.e., with a higher U/t value, one can achieve a high-energy transition, but at the expense of transition strength. Figure 2(b) shows that at a low U/t limit, the whole spectrum is redshifted, with a lesser number of widely separated bright states. On the other hand, at a high U/t limit, the whole spectrum is blueshifted, with a greater number of closely spaced bright states and many transitions of moderate to good oscillator strengths. At a high U/t interaction, degeneracy of some dark states is lifted, resulting in some states having favorable parity for an optical transition. These kinds of closely spaced bright states can be interesting for the possibility of coherent excitation.

We have looked into how the delocalized states and the transition strength can be tuned through the implementation of chemical doping of nitrogen and/or boron in GQD. The key role is played by the partial dipole–partial dipole

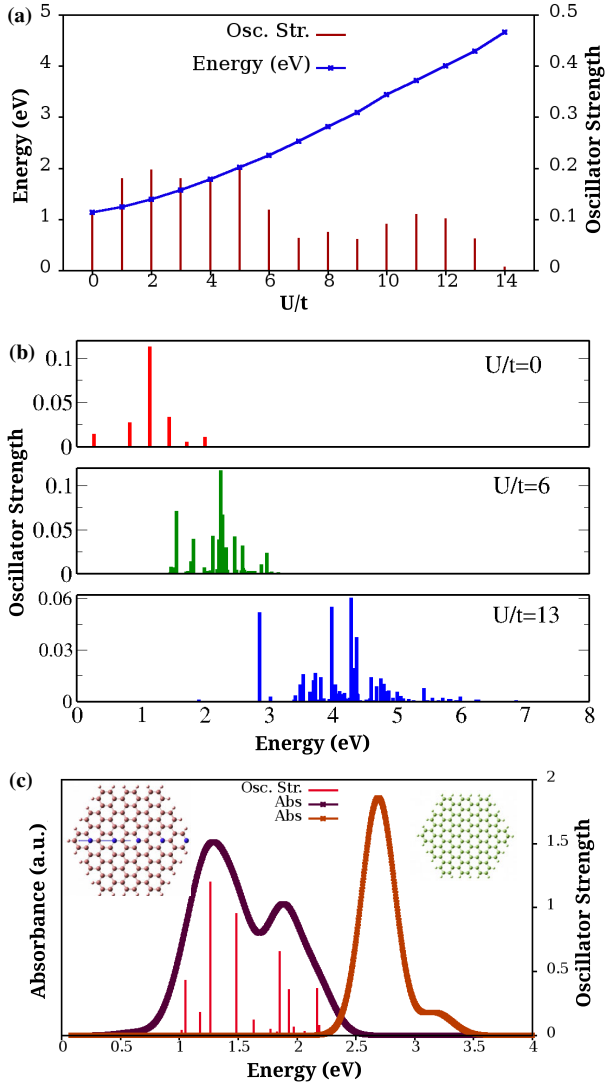

FIG. 2. (a) Variation of oscillator strength (×10) and absorption energy of acene GQDs with C30 at different U/t values in a many-body calculation. (b) The transition-energy states get more blueshifted and become more closely spaced having a greater number of states moderate to high oscillator strength (×10) at a high U/t ratio, whereas for a low U/t value, bright states are redshifted and are more separated. (c) Emergence of high oscillator strength at the near-IR region due to partial dipole–partial dipole coupling in substituted GQDs.

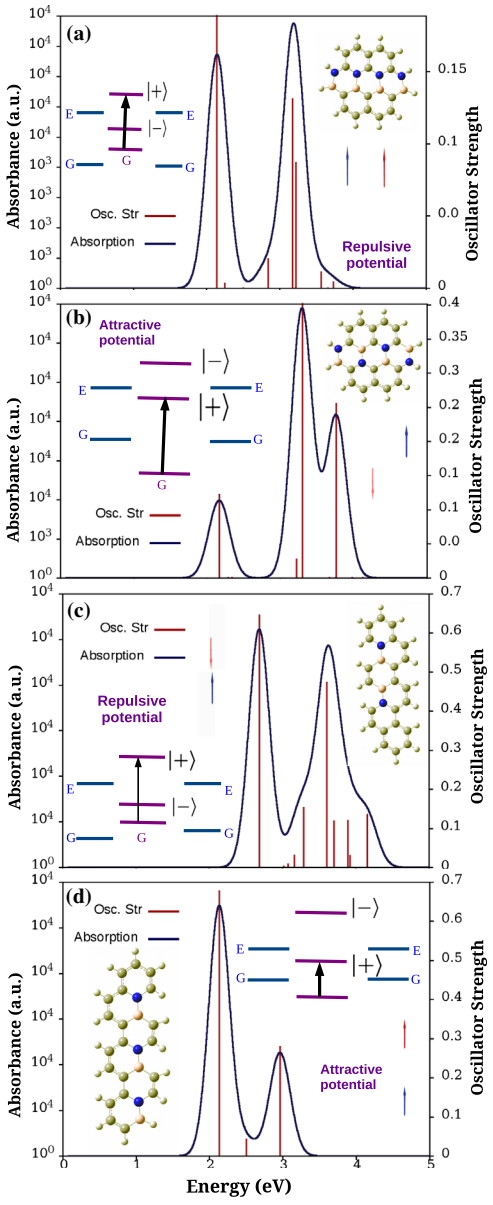

FIG. 3. The orientation of boron and nitrogen in GQDs dictates the alignments of partial dipoles, resulting in either an attractive or a repulsive potential of dipolar coupling. Our DFT calculations show that, for an attractive partial dipole–partial dipole potential, the coherent states are more redshifted than the incoherent states, whereas for a repulsive potential, the incoherent states are in the red end to result either repulsive (a),(c) or attractive (b),(d) potential of dipolar coupling.

coupling. Figures 2(c) and 3 show how the different types of orientations for the B and N substitution can control the alignment of the partial dipoles to produce either an attractive or a repulsive potential of dipolar coupling and can result in high oscillator strength at a new energy. Figure 3 shows the structures of the GQDs along with their partial dipole alignment, as well as the transition energy and strength obtained from the DFT calculations. For the same structures, the CI calculations are shown in Fig. 4(a) in the same sequence. For some other structures and larger GQDs, the results of the many-body, DFT, and semi-empirical calculations are shown in the SM [47]. The Fig. 3 insets show the schematic of a two-state model for dipolar coupling, i.e., Davydov splittings, where the relative position of the coherent and incoherent states are obtained from DFT calculations, presented in Tables II and III (see also the SM [47] for other structures). Davydov splitting is mainly discussed in the aggregate types of systems [49],

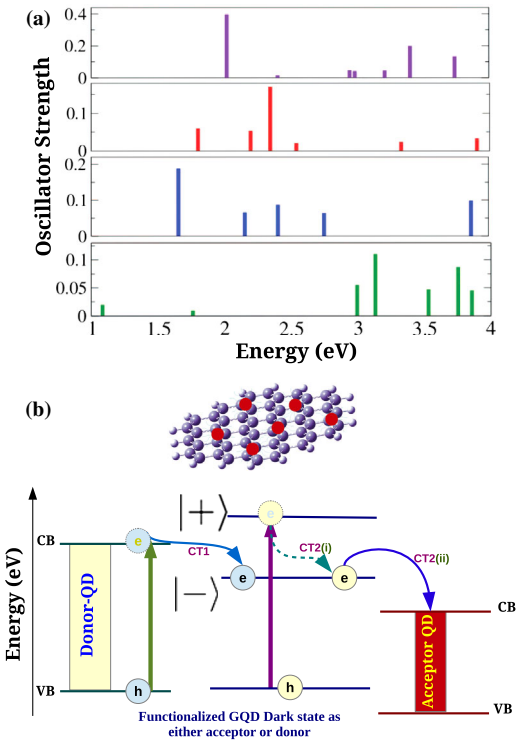

FIG. 4. (a) For the same sequence of GQD shown in Fig. 3, the optical transition determined by a many-body calculation depends, in a similar fashion, on DFT. The emergence of high oscillator strength (×10) in the lower energy is observed due to the dipole-dipole interaction. (b) Schematic of the hybrid QDs and energy states involved in the electron transfer. The relative position of the dark state at lower energy compared to the bright state in GQDs can make the composite efficient in electron transfer by taking either an electron from another excited QD (CT1) or for GQD excitation. An electron from the bright state can go through phonon relaxation to the dark state [CT2(i)], prohibiting the radiative loss and enhancing the electron transfer [CT2(ii)].

TABLE II. For the GQDs shown in Fig 3(a)—i.e., chemical doped GQDs with a repulsive potential—the transition energy, the states involved for the transitions (with their percentages of contribution in parentheses), transition dipoles with their representative directions, and the resulting oscillator strengths are presented.

Energy (eV)	States involved	Tr. dipole (a.u.)	Osc. str.
3.18 [blueshifted	76–79 (57)	0.534 22↑	0.1308
coherent (β)]	78–81 (29)	0.382 23↑	
2.84 [redshifted	78–81 (62)	0.555 34↑	0.02
incoherent (α)]	76–79 (32)	−0.401 10↓	
2.14 (edge state)	78–79 (96)	0.691 49↑	0.1885

where the quasiclassical vector treatment and the electrostatic interaction between the transition moment dictates the splitting energy between the coherent and incoherent states (see the SM [47]). Interestingly, here we also find a similar kind of splitting due to the partial dipole–partial dipole coupling in doped GQD systems. Our DFT calculations on GQDs give the relative position of coherent and incoherent states in the same way as in the quasiclassical vector-model treatment for aggregates. Table II and III reflect the states involved and their contribution to the transition dipoles for either attractive or repulsive potentials for two GQDs; for a higher number of GQDs, see the SM [47]. For the attractive dipolar coupling, the constructive interfering states get shifted to lower energies compared to the destructive interfering states. In the case of repulsive dipolar coupling, the dark states get redshifted. It is interesting to note that, in the case of the substitution here, the edge-state contributions are also enhanced. They are not merely dictated by the boundary condition of the GQDs, but also by the nature of the chemical doping. The many-body calculation with the extended Hubbard model Hamiltonian shows effects that are qualitatively similar to those observed with DFT calculations. The emergence of high oscillator strength at the red end is also observed here, depending on the attractive dipole-dipole interactions. Thus, in the substituted GQDs for attractive potential, the bright states are more redshifted than the dark states,

TABLE III. For the GQDs shown in Fig. 3(d)—i.e., chemical doped GQDs with attractive potential—the transition energy, the states involved for the transitions (with their percentages of contribution in parentheses), transition dipoles with their representative directions, and the resulting oscillator strengths are presented.

Energy (eV)	States involved	Tr. dipole (a.u.)	Osc. str.
2.96 [redshifted	85–87 (50)	0.497 58↑	0.2796
coherent (β)]	86–89 (48)	0.492 43↑	
3,27 [blueshifted	85–87 (44)	0.468 23↑	0.0203
incoherent (α)]	86–89 (42)	−0.460 64↓	
2.13 (edges state)	86 to 87 (100)	0.705 57↑	0.6766

where, as for the repulsive potential, dark states are generated at the red end. Interestingly, experimentalists are using group IV-VI quantum dots along with graphene matrix or graphene quantum dots to prepare hybrid quantum-dot nanofilms where one acts as a donor and the other as an acceptor, while also looking for their electron-transfer dynamics [50,51]. Efficient electron transfer can dramatically increase photocurrent generation in the hybrid-QD-sensitized solar cells. In fact, when a graphene quantum dot is photoexcited, the exciton generated needs to migrate to the donor-acceptor interface to dissociate. Energy transfer can occur through either a dipole-dipole interaction or an electron-exchange interaction. Energy transfer through an electron-exchange interaction (which requires orbital overlap; the Dexter mechanism) and energy transfer through a dipole-dipole interaction (the Förster mechanism) are shown in the equations below [52–54]. In the exchange mechanism, the rate of energy transfer decreases exponentially with the increase in donor-acceptor distance (0.1–1 nm), whereas, through the dipole-dipole interaction, energy transfer can occur over a long range (1–10 nm):

$$
\begin{aligned}
D^* + A &\rightarrow D + A^* \\
k_{\text{exchange}} &\propto |\langle \psi^*(D)\psi(A)|H_{\text{ex}}|\psi(D)\psi^*(A)\rangle|^2 \\
H_{\text{ex}} &\propto e^{-R_{DA}} \\
k_{\text{dipdip}} &\propto |\langle \psi^*(D)\psi(A)|H_{\text{dipdip}}|\psi(D)\psi^*(A)\rangle|^2 \\
H_{\text{dipdip}} &\propto \frac{\mu_D^* \mu_A^*}{R_{DA}^3}.
\end{aligned}
$$

Now, as we have shown, engineering the GQDs by site-specific chemical doping, one can introduce the dipolar interaction in a controlled manner to get red-end dark states that are important for an efficient electron transfer and that can be used for a GQD-sensitized solar cell. In Fig. 4(b), we present a schematic of electron transfer and charge separation in a GQD-QD composite and show how the red-end incoherent state facilitates electron transfer.

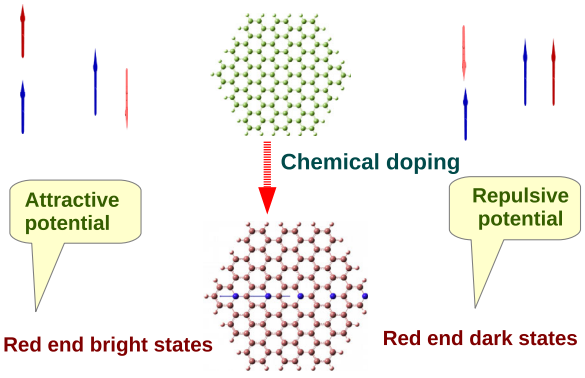

FIG. 5. Schematic showing, in substituted GQDs, that the attractive dipolar kind of potential will move the coherent state in the red end relative to the incoherent state, whereas the repulsive dipolar kind of potential will operate in the reverse manner.

Here, in either CT1 pathway, the dark state of the doped GQD can accept the electron from a photoexcited donor QD or, in the CT2 pathway, the photoexcited GQD can relax to the dark state, followed by an efficient electron transfer to another acceptor QD, resulting in efficient charge separation. Again, the bright state can also be tuned to high oscillator strength for enhanced photonic activity. Thus, we can employ the dipolar kind of potential in a doped GQD to tune the relative position of bright and dark states, as is shown schematically in Fig. 5.

IV. CONCLUSIONS

Our studies establish that controlling the coherent superposition of quantum states high oscillator strength in desirable energy can be achieved through partial dipole–partial dipole interactions in substituted graphene quantum dots. Our DFT and many-body calculations show that, in substituted GQDs, due to the coupling among the partial dipoles, the Davydov type of splitting is obtained in the same fashion as is observed with the quasiclassical vector treatment of dipolar coupling in aggregates. We show that, in an attractive dipolar potential, the bright state in functionalized GQDs is more redshifted compared to its dark counterpart. However, the repulsive dipolar potential produces a dark-state red end which can be used for an efficient electron transfer, as was reported previously [39,40].

Experimentalists have reported efficient electron transfer in the low-lying dark state of nanostructured graphene from group IV-VI quantum dots [50,51]. Hence, utilizing partial dipole–partial dipole coupling, a proper architecture of the dark state in GQDs, relative to the other QDs in a hybrid QD, can be achieved. This achievement would pave the way for an efficient electron transfer. Again, our results reflect that the nonadditive edge-state transition can be enhanced through the functionalization of GQDs. Also, our studies reveal that the effect of strain can change the U/t ratio, creating more closely spaced bright states, which are important for coherent excitation.

ACKNOWLEDGMENTS

We thank Dr. A. Pati, Dr. S. S. R. K. C. Yamijala, and Ms. S. Banerjee for the discussions. S. K. P. acknowledges Department of Science and Technology, Ministry of Science and Technology for the funding. B. P. acknowledges the support of a University Grants Commission fellowship.

[1] C. R. Dean, A. F. Young, I. Meric, C. Lee, L. Wang, S. Sorgenfrei, K. Watanabe, T. Taniguchi, P. Kim, K. L. Shepard, and J. Hone, Boron nitride substrates for high-quality graphene electronics, Nat. Nanotechnol. **5**, 722 (2010).

[2] K. F. Mak, C. Lee, J. Hone, J. Shan, and T. F. Heinz, Atomically Thin MoS_2: A New Direct-Gap Semiconductor, Phys. Rev. Lett. **105**, 136805 (2010).

[3] O. Lopez-Sanchez, D. Kayci, M. Radenovic, and A. A. Kis, Ultra-sensitive photo-detectors based on mono-layer MoS_2 Lembke, Nat. Nanotechnol. **8**, 497 (2013).

[4] L. Britnell, R. M. Ribeiro, A. Eckmann, R. Jalil, B. D. Belle, A. Mishchenko, Y.-J. Kim, R. V. Gorbachev, T. Georgiou, S. V. Morozov, A. N. Grigorenko, A. K. Geim, C. Casiraghi, A. H. Castro Neto, and K. S. Novoselov, Strong light-matter interactions in heterostructures of atomically thin films, Science **340**, 1311 (2013).

[5] M. Liu, X. Yin, E. Ulin-Avila, B. Geng, T. Zentgraf, L.Ju. Wang, and X. Zhang, A graphene-based broadband optical modulator, Nature (London) **474**, 64 (2011).

[6] A. N. Grigorenko, M. Polini, and K. S. Novoselov, Graphene plasmonics, Nat. Photonics **6**, 749 (2012).

[7] E. Towe, T. Palacios, and M. Suemitsu, Emerging graphene-based electronic and photonic devices, circuits, and systems, Proc. IEEE **101**, 1518 (2013).

[8] D. Ansell, I. P. Radko, Z. Han, F. J. Rodriguez, S. I. Bozhevolnyi, and A. N. Grigorenko, Hybrid graphene plasmonic waveguide modulators, Nat. Commun. **6**, 8846 (2015).

[9] Q. Bao and K. P. Loh, Graphene photonics, plasmonics, and broadband optoelectronic devices, ACS Nano **6**, 3677 (2012).

[10] B. Vasic and R. Gajic, Graphene-Covered Photonic Structures for Optical Chemical Sensing., Phys. Rev. Applied **4**, 024007 (2015).

[11] K. Nakada, M. Fujita, G. Dresselhaus, and M. S. Dresselhaus, Edge state in graphene ribbons: Nanometer size effect and edge shape dependence, Phys. Rev. B **54**, 17954 (1996).

[12] Y. Li, H. Shu, S. Wang, and J. Wang, Electronic and optical properties of graphene quantum dots: The role of many-body effects, J. Phys. Chem. C **119**, 4983 (2015).

[13] P. Moon and M. Koshino, Optical absorption in twisted bilayer graphene, Phys. Rev. B **87**, 205404 (2013).

[14] V. Georgakilas, M. Otyepka, A. B. Bourlinos, V. Chandra, N. Kim, K. C. Kemp, P. Hobza, R. Zboril, and K. S. Kim, Functionalization of graphene: Covalent and non-covalent approaches, derivatives and applications, Chem. Rev. **112**, 6156 (2012).

[15] D. Kozawa, X. Zhu, Y. Miyauchi, S. Mouri, M. Ichida, H. Su, and K. Matsuda, Excitonic photoluminescence from nanodisc states in graphene oxides, J. Phys. Chem. Lett. **5**, 1754 (2014).

[16] J. O. Sofo, A. S. Chaudhari, and G. D. Barber, Graphane: A two-dimensional hydrocarbon, Phys. Rev. B **75**, 153401 (2007).

[17] A. Lherbier, X. Blase, Y. M. Niquet, F. Triozon, and S. Roche, Charge Transport in Chemically Doped 2D Graphene, Phys. Rev. Lett. **101**, 036808 (2008).

[18] T. B. Martins, R. H. Miwa, A. J. R. da Silva, and A. Fazzio, Electronic and Transport Properties of Boron-Doped Graphene Nanoribbons, Phys. Rev. Lett. **98**, 196803 (2007).

[19] R. J. Koch, M. Weser, W. Zhao, F. Vines, K. Gotterbarm, S. M. Kozlov, O. Hofert, M. Ostler, C. Papp, J. Gebhardt, H. P. Steinruck, A. Gorling, and Th. Seyller, Growth and electronic structure of nitrogen-doped graphene on Ni(111), Phys. Rev. B **86**, 075401 (2012).

[20] D. Usachov, O. Vilkov, A. Gruneis, D. Haberer, A. Fedorov, V. K. Adamchuk, A. B. Preobrajenski, P. Dudin, A. Barinov, M. Oehzelt, C. Laubschat, and D. V. Vyalikh, Nitrogen-doped graphene: Efficient growth, structure, and electronic properties, Nano Lett. **11**, 5401 (2011).

[21] F. Joucken, Y. Tison, J. Lagoute, J. Dumont, D. Cabosart, B. Zheng, V. Repain, C. Chacon, Y. Girard, A. R. Botello-Mendez, S. Rousset, R. Sporken, J. C. Charlier, and L. Henrard, Localized state and charge transfer in nitrogen-doped graphene, Phys. Rev. B **85**, 161408(R) (2012).

[22] L. Zhao, R. He, K. T. Rim, T. Schiros, K. S. Kim, H. Zhou, C. Gutirrez, S. P. Chockalingam, C. J. Arguello, L. Plov, D. Nordlund, M. S. Hybertsen, D. R. Reichman, T. F. Heinz, P. Kim, A. Pinczuk, G. W. Flynn, and A. N. Pasupathy, Visualizing individual nitrogen dopants in monolayer graphene, Science **333**, 999 (2011).

[23] L. Yang, J. Deslippe, C.-H. Park, M. L. Cohen, and S. G. Louie, Excitonic Effects on the Optical Response of Graphene and Bilayer Graphene, Phys. Rev. Lett. **103**, 186802 (2009).

[24] L. A. Ponomarenko, F. Schedin, M. I. Katsnelson, R. Yang, E. W. Hill, K. S. Novoselov, and A. K. Geim, Chaotic Dirac billiard in graphene quantum dots, Science **320**, 356 (2008).

[25] M. Grujic, M. Zarenia, A. Chaves, M. Tadic, G. A. Farias, and F. M. Peeters, Electronic and optical properties of a circular graphene quantum dot in a magnetic field: Influence of the boundary conditions, Phys. Rev. B **84**, 205441 (2011).

[26] A. V. Rozhkov, G. Giavaras, Y. P. Bliokh, V. Freilikher, and F. Nori, Electronic properties of mesoscopic graphene structures: Charge confinement and control of spin and charge transport, Phys. Rep. **503**, 77 (2011).

[27] T. Basak, H. Chakraborty, and A. Shukla, Theory of linear optical absorption in diamond-shaped graphene quantum dots, Phys. Rev. B **92**, 205404 (2015).

[28] S. S. R. K. C. Yamijala, A. Bandyopadhyay, and S. K. Pati, Electronic properties of zigzag, armchair and their hybrid quantum dots of graphene and boron-nitride with and without substitution: A DFT study, Chem. Phys. Lett. **603**, 28 (2014).

[29] Deepika, T. J. D. Kumar, A. Shukla, and R. Kumar, Edge configurational effect on band gaps in graphene nanoribbons, Phys. Rev. B **91**, 115428 (2015).

[30] Y. Kobayashi, K. I. Fukui, T. Enoki, K. Kusakabe, and Y. Kaburagi, Observation of zigzag and armchair edges of graphite using scanning tunneling microscopy and spectroscopy, Phys. Rev. B **71**, 193406 (2005).

[31] P. Potasz, A. D. Guclu, A. Wojs, and P. Hawrylak, Electronic properties of gated triangular graphene quantum dots: Magnetism, correlations, and geometrical effects, Phys. Rev. B **85**, 075431 (2012).

[32] Karol Szaowski, Electric field control of the indirect magnetic coupling through a short graphene nanoribbon, Phys. Rev. B **90**, 085410 (2014).

[33] P. Potasz, A. D. Guclu, A. Wojs, and P. Hawrylak, Zero-energy states in triangular and trapezoidal graphene structures, Phys. Rev. B **81**, 033403 (2010).

[34] H. Tetsuka, R. Asahi, A. Nagoya, K. Okamoto, I. Tajima, R. Ohta, and A. Okamoto, Optically tunable amino-functionalized graphene quantum dots, Adv. Mater. **24**, 5333 (2012).

[35] P. Sony and A. Shukla, Large-scale correlated calculations of linear optical absorption and low-lying excited states of

polyacenes: Pariser-Parr-Pople Hamiltonian, Phys. Rev. B **75**, 155208 (2007).
[36] E. B. Guidez and C. M. Aikens, Origin and TDDFT benchmarking of the plasmon resonance in acenes, J. Phys. Chem. C **117**, 21466 (2013).
[37] D. Beljonne, H. Yamagata, J. L. Bredas, F. C. Spano, and Y. Olivier, Charge-Transfer Excitations Steer the Davydov Splitting and Mediate Singlet Exciton Fission in Pentacene, Phys. Rev. Lett. **110**, 226402 (2013).
[38] A. Chernikov, O. Yaffe, B. Kumar, Y. Zhong, C. Nuckolls, and T. F. Heinz, Spectroscopic study of anisotropic excitons in single crystal hexacene, J. Phys. Chem. Lett. **5**, 3632 (2014).
[39] C. Creatore, M. A. Parker, S. Emmott, and A. W. Chin, Efficient Biologically Inspired Photocell Enhanced by Delocalized Quantum States, Phys. Rev. Lett. **111**, 253601 (2013).
[40] Y. Zhang, S. Oh, F. H. Alharbi, G. S. Engel, and S. Kais, Delocalized quantum states enhance photocell efficiency, Phys. Chem. Chem. Phys. **17**, 5743 (2015).
[41] C. Raghu, Y. Anusooya Pati, and S. Ramasesha, Density-matrix renormalization-group study of low-lying excitations of polyacene within a Pariser-Parr-Pople model, Phys. Rev. B **66**, 035116 (2002).
[42] S. Dutta, S. Lakshmi, and S. K. Pati, Electron-electron interactions on the edge states of graphene: A many-body configuration interaction study, Phys. Rev. B **77**, 073412 (2008).
[43] K. Ohno, Some remarks on the Pariser-Parr-Pople method, Theor. Chim. Acta **2**, 219 (1964).
[44] A. Datta and S. K. Pati, Dipolar interactions and hydrogen bonding in supramolecular aggregates: Understanding cooperative phenomena for 1st hyperpolarizability, Chem. Soc. Rev. **35**, 1305 (2006).
[45] T. Ohgoe, T. Suzuki, and N. Kawashima, Quantum phases of hard-core bosons on two-dimensional lattices with anisotropic dipole-dipole interaction, Phys. Rev. A **86**, 063635 (2012).
[46] R. Korytár, D. Xenioti, P. Schmitteckert, M. Alouani, and F. Evers, Signature of the Dirac cone in the properties of linear oligoacenes, Nat. Commun. **5**, 5000 (2014).
[47] See Supplemental Material at http://link.aps.org/supplemental/10.1103/PhysRevApplied.6.044014 for additional supporting results.
[48] S. S. R. K. C. Yamijala, M. Mukhopadhyay, and S. K. Pati, Linear and nonlinear optical properties of graphene quantum dots: A computational study, J. Phys. Chem. C **119**, 12079 (2015).
[49] H. Yamagata, D. S. Maxwell, J. Fan, K. R. Kittilstved, A. L. Briseno, M. D. Barnes, and F. C. Spano, HJ-aggregate behavior of crystalline 7,8,15,16-tetraazaterrylene: Introducing a new design paradigm for organic materials, J. Phys. Chem. C **118**, 28842 (2014).
[50] N. Zhu, K. Zheng, K. J. Karki, M. Abdellah, Q. Zhu, S. Carlson, D. Haase, K. Žídek, J. Ulstrup, S. E. Canton, T. Pullerits, and Q. Chi, Sandwiched confinement of quantum dots in graphene matrix for efficient electron transfer and photocurrent production, Sci. Rep. **5**, 9860 (2015).
[51] I. V. Lightcap and P. V. Kamat, Graphitic design: Prospects of graphene-based nanocomposites for solar energy conversion, storage, and sensing, Acc. Chem. Res. **46**, 2235 (2013).
[52] T. Förster, Transfer mechanisms of electronic excitation energy, Radiation Research Supplement **2**, 326 (1960).
[53] D. L. Dexter, A theory of sensitized luminescence in solids, J. Chem. Phys. **21**, 836 (1953).
[54] A. Olaya-Castro and G. D. Scholes, Energy transfer from Förster Dexter theory to quantum coherent light harvesting, Int. Rev. Phys. Chem. **30**, 49 (2011).